ROYAL SOCIETY
OF CHEMISTRY

Check for updates

Delayed photodissociation of the tin cluster Sn_{22}^-

Alexander Jankowski, [iD] *[a] Paul Fischer, [iD] [a] Klavs Hansen [iD] [b] and Lutz Schweikhard[a]

Millisecond-delayed photodissociation of gas-phase Sn_{22}^- clusters stored in a Penning trap is investigated as a function of excitation energy. Sn_{15}^- is the only significant charged fragment, indicative of the break-off of neutral heptamers. Fits of the time-resolved fragmentation require a distribution of decay constants, caused by the finite width of the internal energy distribution of the cluster ensemble prior to photoexcitation. A lower limit for the dissociation energy for the loss of Sn_7 is determined to be 2.1(1) eV, a factor of two above literature quantum chemical calculations.

1 Introduction

The reactivity of isolated molecules and clusters is of prime importance for the quantitative understanding of a number of questions ranging from stabilities in molecular beams to abundances in the interstellar medium. The characteristics of thermal decays is one of these questions. Most metal clusters decay by emission of monomers or dimers.[1–3] However, elements close to the bulk metal-nonmetal boundary behave differently. Prominent examples are clusters of group-14 elements—carbon, silicon, germanium, tin, and lead. The interatomic bonds of small clusters formed from these elements are more directional and less metallic than those of, *e.g.*, alkali or coinage metals. This is observed, for example, in ion-mobility measurements, where deviations from spherical structures can be matched to less metallic bonding.[4] The non-metallic nature of the bonds is also reflected in the more complex fragmentation patterns of such clusters. In particular, the break-off of polyatomic fragments has been observed for singly-charged carbon[5–8] as well as silicon[9–13] and germanium clusters,[11,12] highlighting their covalent nature. This matches the elements' bulk classification as nonmetal (C) and metalloids (Si, Ge).

The structures of clusters formed from tin, which is characterized as a metal in the bulk, are of great interest, both theoretical and experimental. Neutral tin clusters Sn_n have been probed by combined electric beam deflection and photodissociation spectroscopy to reveal their geometric structures and optical absorption properties,[14] as well as by photo-induced ionization to determine ionization thresholds.[15] For the anionic species Sn_n^-, photoelectron spectroscopy (PES) has been performed to find the electron affinities[16–19] as well as the HOMO–LUMO gaps of those clusters.[18,19] Collision-induced dissociation and trapped-ion electron diffraction has been applied to both anionic Sn_n^- and cationic Sn_n^+ clusters, alongside density-functional theory (DFT) calculations as probes of the dissociation pathways and their energy thresholds.[20–22] Furthermore, ion-mobility measurements have been performed to investigate the structure of Sn_n^+ clusters, as well as their melting point,[23,24] and surface-induced dissociation was performed to investigate their dissociation pathways.[25] DFT calculations have been performed for neutral and singly-charged cations and anions[20–22,26–31] to determine geometric and electronic properties. Similar to Pb_n^{2-}, doubly-charged Sn_n^{2-} clusters have been found experimentally to decay by fission into two singly-charged smaller clusters at size ranges up to $n \simeq 50$,[32,33] further highlighting the exceptional characteristics of these two elements. Tin also has potential applications as feedstock for the highly-charged atomic tin ions that can provide the XUV light needed for the increasingly smaller sizes aimed for in nanodevice lithography.[34]

Here, the decay of the photoexcited singly-charged cluster Sn_{22}^- is investigated in the gas phase. The cluster is found to decay by break-off of a neutral tin heptamer:

$$Sn_{22}^- \rightarrow Sn_{15}^- + Sn_7. \tag{1}$$
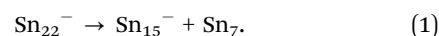
Following the procedure of previous experiments[35,36] the decay is monitored as a function of time after photoexcitation with various photon energies. The observed shifts in the time-depended decay, and thus the decay-constant distribution, are used to derive the energy distribution of the cluster ensemble and the dissociation energy of Sn_{22}^-. Such activation energies are notoriously difficult to determine experimentally. The result we will find here is a lower limit which is a factor of two higher

[a] *Institute for Physics, University of Greifswald, Felix-Hausdorff-Straße 6, 17498 Greifswald, Germany. E-mail: alexander.jankowski@uni-greifswald.de*

[b] *Center for Joint Quantum Studies and Department of Physics, School of Science, Tianjin University, 92 Weijin Road, Tianjin 300072, China*

This journal is © the Owner Societies 2024

Phys. Chem. Chem. Phys., 2024, **26**, 1105–1112 | **1105**

than the value calculated by quantum chemical methods. It therefore provides a possibility to calibrate the theoretical methods for the fairly large electron number system (Sn_{22}^{-} has 1101 electrons).

An important and directly observable phenomenon in the experiments is the width of the distribution of rate constants. This width in turn reflects the width of the thermal energy distribution of the clusters prior to the pulsed laser excitation. The energy distribution will be shown to be slightly above the thermal distribution defined by the trap temperature. The increase is due to the hyperthermal motion of the charged particles in the trap. The finding is important given the wide-spread use of traps as collection and thermalization devices for which much still remains to be understood. The present results will contribute with fitted effective temperatures to the future model building of the topic.

2 Experimental procedure

The experiments were performed at the ClusterTrap setup,[37,38] where delayed reactions after photoexcitation of clusters have previously been studied for gold,[39,51] silver,[40] vanadium,[41,42] and lead.[36] The gas-phase reactions were performed in a 12-Tesla Penning trap, where a pulsed laser beam was axially guided through the trap for photoexcitation. The details of the specific experimental procedure used here are described in the following.

Anionic tin clusters were produced in a pulsed laser-ablation source[43] (pulse rate of 10 Hz) with cluster condensation in helium, producing singly-charged anionic tin clusters. These were captured in a linear Paul trap with argon buffer gas at a pressure of around 10^{-3} mbar. After accumulation of typically ten cluster pulses, the ion ensemble was transferred into the Penning trap. Here, the cluster ions were exposed to argon gas pulsed into the trap volume through a piezoelectric valve, to a peak pressure of 10^{-6} mbar, as measured outside of the magnet. The collisions with the gas atoms dampened the axial oscillations along the magnetic field lines and their perpendicular cyclotron motion.

To record the distribution of ion species stored in the trap at a given time, all ions were ejected towards a multichannel-plate ion detector and a time-of-flight (ToF) spectrum was recorded. Such a spectrum is shown in Fig. 1(a). The distribution of cluster sizes observed between $n \approx 14$ and $n \approx 32$ is determined by the parameters chosen for the source, the Paul trap acceptance, the timing for the transfer section, and the Penning-trap capture process. In addition, some smaller clusters resulted from collision-induced dissociation during capture and cooling of the cluster ions. Note that, already in this spectrum, in addition to the smaller clusters Sn_9^- and Sn_{10}^-, Sn_{15}^- was present with a prominent intensity.

For photoexcitation studies, a mass-selective process needs to be employed to ensure that only a single species of interest is present in the trap. To that end, all ions were excited with respect to their magnetron motion, resulting in an increased
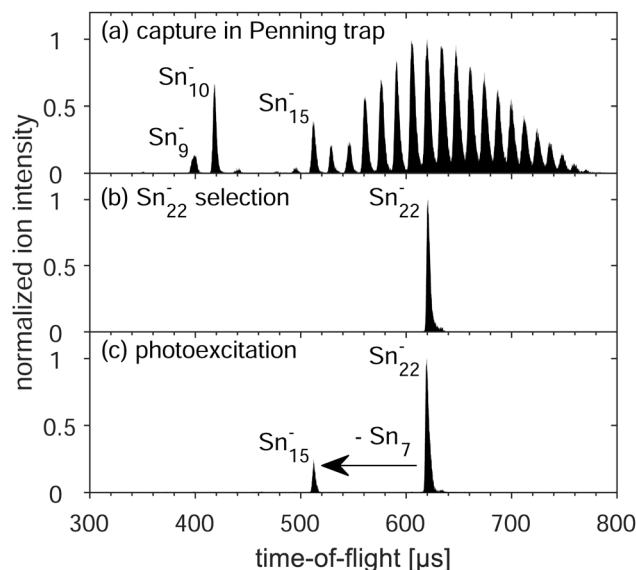

Fig. 1 Time-of-flight spectra (each normalized to its highest signal) of tin clusters (a) after their capture and buffer-gas cooling of the ion motion, (b) after mass selection of Sn_{22}^-, and (c) after photoexcitation with 2.48 eV photons and ion ejection after a delay of one second.

magnetron radius.[44] Quadrupolar excitation at the frequency of the cyclotron motion of the cluster species to be retained was applied for mass-to-charge selective conversion of magnetron into cyclotron motion.[45] In combination with the buffer-gas collisions, this led to the axialization of the Sn_{22}^- clusters[46,47] (Fig. 1(b)). This mass-selection procedure took about two seconds.

After the Sn_{22}^- precursor selection, the argon gas was pumped from the trap for half a second before the clusters were irradiated by a pulsed nanosecond laser and ejected for time-of-flight analysis (Fig. 1(c)). The delay time between photo-excitation and ion ejection was varied between 25 microseconds and a second with a logarithmic spacing between the 24 measuring points. The finite time it takes to accelerate the ions out of the trap limits the accessible times to longer than 25 microseconds. On the other hand, at delay times above a second, additional cooling effects, e.g. radiative or buffer-gas cooling, have to be considered. For the photoexcitation, a nanosecond pulse from an OPO laser system (EKSPLA NT342B) was used with pulse energies between 5 and 10 millijoules at wavelengths λ = 410, 430, 450, 475, 500, 525, 550 and 595 nm, i.e. photon energies E_{ph} ranging from 3.0 eV to 2.1 eV. This range leads to delayed fragmentation processes observable within the time frame mentioned above. The laser-beam diameter was d = 1.7 cm at the center of the Penning trap, fully irradiating the stored cluster ensemble. A uniform photon-density distribution is assumed for the laser beam profile as an approximation to the higher order Laguerre–Gaussian mode at which the laser operates.

The number of Sn_{22}^- precursors per experimental cycle was between 100 and 200. For a given wavelength and delay, the cycle was repeated 20 to 30 times to increase statistics. Additionally, a reference ToF spectrum without application of the laser pulse (similar to the spectrum in Fig. 1(b)) was recorded

1106 | *Phys. Chem. Chem. Phys.*, 2024, **26**, 1105–1112

This journal is © the Owner Societies 2024

interleaved for subtraction of a small amount of background counts, not visible in the linear vertical scaling of Fig. 1.

3 Experimental results

In the following, spectra such as the one of Fig. 1(c) are analysed with respect to the fragmentation yield of Sn_{15}^- as a function of the excitation pulse energy in Section 3.1 and as a function of time and photon energy in Section 3.2.

3.1 Yield as a function of excitation pulse energy

For best reliability of the time- and wavelength-resolved measurements in the present study, restriction to regimes of predominantly single-photon absorption is crucial. To ensure this, measurements were first performed at different excitation-laser pulse energies E_{pulse}, from 0.35 to 6.5 mJ, for a fixed photon energy of $E_{ph} = 2.33$ eV and fixed delay time of a second. The resulting data (Fig. 2) are well described by a linear function through the origin, which indicates that fragmentation occurs after absorption of a single photon in this pulse-energy regime. In particular, there is no indication of the positive curvature one expects from higher-order processes. Fitting the yield $Y(E_{pulse}) = \alpha E_{pulse}$ to the data results in a slope of $\alpha = 15.6(6)$ J^{-1}. Thus, the photoabsorption cross section σ_{ph} at this wavelength of 532 nm is

$$\sigma_{ph} = \alpha h \nu \pi \frac{d^2}{4} = 1.32(5) \times 10^{-21} \text{m}^2, \quad (2)$$

where h is the Planck constant and ν the frequency of the absorbed photon. The observed fragment yields for the other probed photon energies were very similar. A relatively modest wavelength dependence of the absorption cross section for different photon energies is expected for collective excitation of the surface-plasmon type well known from small metal clusters.[48–50] The dominant single-photon absorption means that the two-photon contribution is small. Fragmentation caused by two-photon absorption will be practically instantaneous with respect to the observation time window of the present experiment, and only result in a small offset in the yield as a function of delay time (see next section).

3.2 Yield as a function of delay time after photo-excitation

Fig. 3 shows the fragment yields Y of Sn_{15}^-, i.e. the observed product of the Sn_{22}^- decay, normalized to all detected ions (i.e. the sum of Sn_{22}^- and Sn_{15}^- ions) as a function of the delay time between photoexcitation and extraction into the time-of-flight mass spectrometer for the photon wavelength of $\lambda = 500$ nm (2.48 eV).

The yields represent the integral of Sn_{15}^- fragments produced from the time of photoexcitation up to ion ejection. Note that the ToF section is linear and clusters that fragment in flight are detected as unfragmented.

The Sn_{15}^- yield rises with increasing delay time, reaching a plateau at the longest times. The blue line in Fig. 3 results from fitting the yield with a single-exponential function of the form

$$Y(t) = \frac{A^2}{2} + A \cdot \left(1 - e^{-k_0 t}\right), \quad (3)$$

where k_0 is the decay constant, A the amplitude, and $A^2/2$ is the offset caused by two-photon absorption. As mentioned above, this offset results from fragmentation occurring at timescales multiple orders of magnitudes shorter than the observation time window of the present setup. The products of this fast fragmentation are, therefore, already detected at the lowest delays probed.

In past investigations, this model function was used to describe the delayed photo-decay of various cluster species at the present setup.[35,36] However, in the present case the fragmentation yield is not well represented by eqn (3), as it is obvious from the fit in Fig. 3 (blue line), where the fitted curve systematically underestimates the yield for short delay times while overestimating it for intermediate delay times. For a better description of the fragment yield, a superposition of
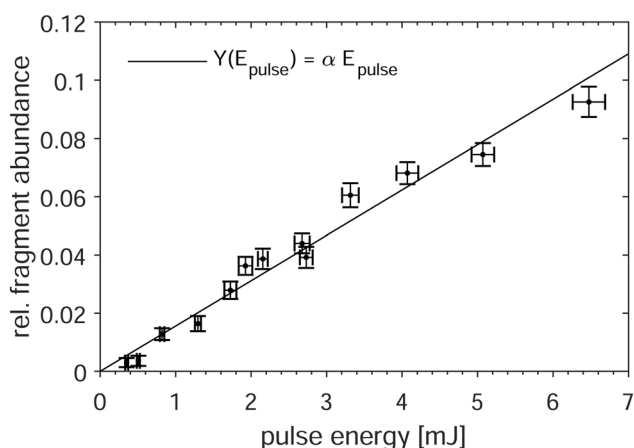
Fig. 2 Relative yield of the Sn_{15}^- fragment as a function of excitation-pulse energy at 532 nm. The horizontal and vertical error bars show the shot-to-shot noise of the laser and the statistical uncertainty of the ion signal, respectively. The solid line is a linear fit.
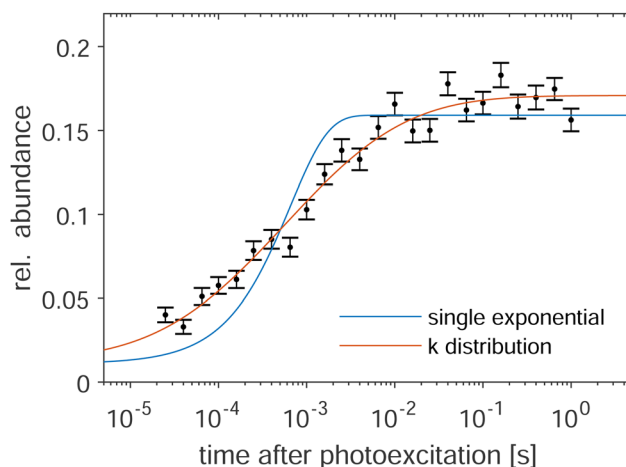
Fig. 3 Relative fragment yield of Sn_{15}^- as a function of delay time for 500 nm photon wavelength. The blue and yellow lines are fits of a single exponential function and of a distribution of such functions, respectively, to the data. For details, see the main text.

This journal is © the Owner Societies 2024

Phys. Chem. Chem. Phys., 2024, **26**, 1105–1112 | **1107**

exponential decays is required. Denoting the decay-constant distribution as $\rho(k)$, the fragment yield becomes

$$Y(t) = \frac{A^2}{2} + A \int_0^\infty \rho(k)\left(1 - e^{-kt}\right)dk. \qquad (4)$$

The distribution is parameterized with a log-normal form

$$\rho(k|k_m, \sigma_k)dk = \frac{1}{\sqrt{2\pi\sigma_k^2}k}\exp\left(-\frac{\left(\ln\frac{k}{k_m}\right)^2}{2\sigma_k^2}\right)dk, \qquad (5)$$

(as motivated in the appendix) with the median k_m and the dimensionless width σ_k. It is used with eqn (4) to model the fragment yields by fitting the parameters A, k_m, and σ_k. The resulting orange line in Fig. 3 shows that the experimental data are much better reproduced than with the single-exponential approach.

Data as in Fig. 3 recorded for other photon energies are shown in Fig. 4. As the precursor preparation is the same for all measurements, the k-distributions, while being different, are connected *via* their identical initial energy distributions prior to the photoabsorption. Therefore, this energy distribution is fitted to the data of all photon energies resulting in a "global" fit and the red lines in Fig. 4. This energy distribution is defined by a single parameter T, the temperature of the initial cluster ensemble, which, together with the clusters' heat capacity, defines the mean internal energy and width of the distribution.

The parameters k_m and σ_k of the distribution function (5) are expressed as

$$k_m\left(E_{ph}|D, T\right) = \omega\exp\left(-\frac{\left(D + E_{0,p} - E_{0,f}\right)(f - 4)}{E_{ph} - D/2 + fk_B T}\right) \text{ and } \quad (6)$$

$$\sigma_k(E_{ph}|D, T) = \frac{\left(D + E_{0,p} - E_{0,f}\right)(f - 4)\sqrt{f}k_B T}{\left(E_{ph} - D/2 + fk_B T\right)^2}, \qquad (7)$$

as motivated in the appendix. Here E_{ph} is the photon energy, ω a frequency factor, f the decaying clusters' number of vibrational degrees of freedom, assumed harmonic, and D their dissociation energy. $E_{0,p/f}$ are the offsets of the caloric curve for the parent and fragment cluster, respectively, in the linear (high temperature) approximation of the Debye model, *i.e.* for canonical values $\langle E \rangle = fk_B T - E_{0,p/f}$. This results in k-distributions where the parameters k_m and σ_k for each curve are replaced by a single set of parameters shared between all yield curves. The curves resulting from the joint fit of all photon energies are also shown in Fig. 4.

Note that—for the chosen photon energies and delay times—there is no observable yield decrease of the Sn_{15}^- cluster signal which would indicate a sequential decay. This suggests that the energy remaining in the clusters after the first fragmentation is not high enough to lead to another decay within the time frame
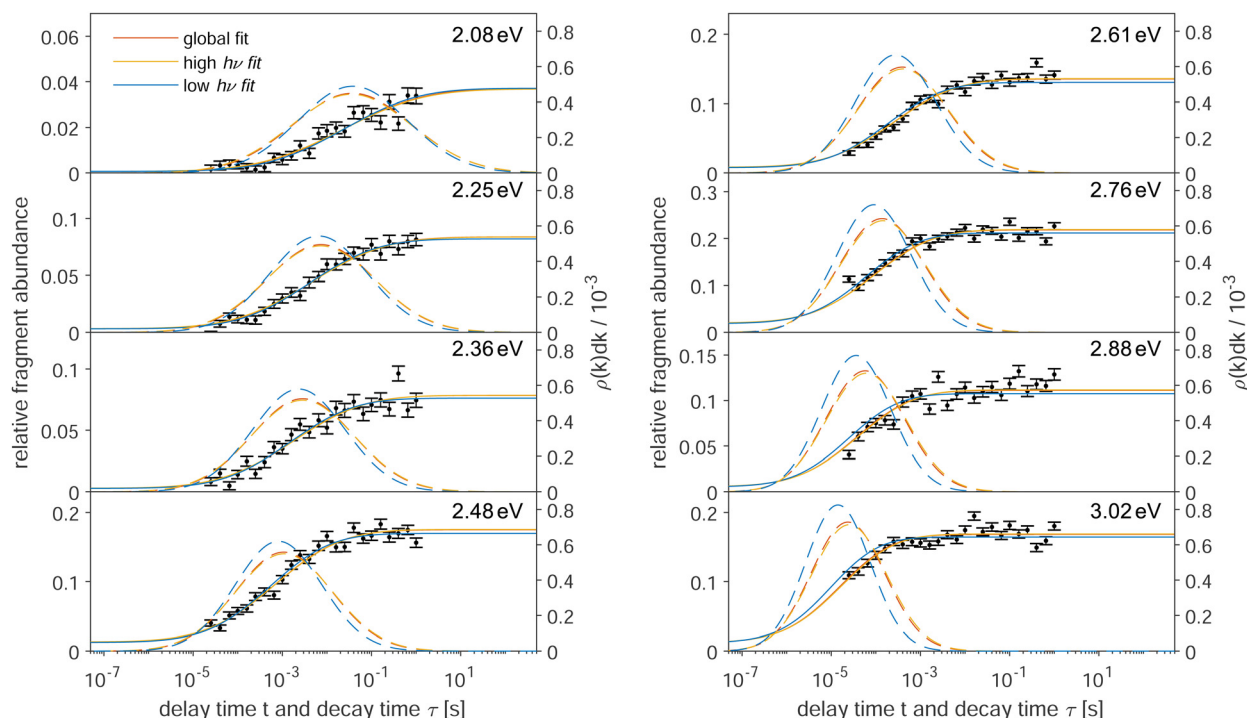
Fig. 4 Relative fragment yield of Sn_{15}^- for various photon wavelengths. The solid lines are fits to the data following a k-distribution. The dashed lines are the k-distributions on a $\tau = 1/k$ axis. The red lines are "global" fits using all measured curves. The almost overlapping yellow lines use the data from the four highest photon energies (2.61 eV to 3.02 eV) for the fit and the blue lines use the data from the four lowest photon energies (2.08 eV to 2.48 eV). The yellow and blue curves for the photon energies, which are not used in their respective fit, are extrapolated. For details, see the main text.

1108 | *Phys. Chem. Chem. Phys.*, 2024, **26**, 1105–1112

This journal is © the Owner Societies 2024

probed in the present study. The observability of such decays has been demonstrated in another study.[36]

4 Discussion

The parameters $f = 60$, $E_{0,\mathrm{p}} - E_{0,\mathrm{f}} = 39$ meV, and $\omega = 2.1 \times 10^{16}$ s^{-1}, approximated as energy independent, are determined as described in the appendix. Thus, only D and T are fitted to the data, together with the individual amplitude values A for the different photon energies. This results in a temperature $T = 460(20)$ K prior to the photoexcitation as well as a dissociation energy $D = 2.1(1)$ eV of Sn$_{22}^-$. As described in the appendix, the frequency factor ω includes an empirically determined factor of 100 on the bulk Debye frequency. To provide an uncertainty estimation for this parameter, the fits are performed without this correction. The resulting dissociation energy is lowered by $\Delta D_\omega = -0.3$ eV, while the temperature stays within the uncertainty of the initial fit, i.e. $\Delta T_\omega < 20$ K. The disregard of the effect of the rotational degrees of freedom for the products in the decay has an unknown effect. It is clear, however, that the effect on D would be positive and that the value quoted is therefore a lower limit.

For the lower photon energies, the fragment yields do not reach the plateau at long delay times, while for the higher photon energies the yields start at times well into the rise of the curve. Thus, in order to check the robustness of the fit, it is also performed using only the data of the four lowest and highest photon energies, i.e. 2.08 eV to 2.48 eV (yellow lines) and 2.61 eV to 3.02 eV (blue lines), respectively. On the one hand, the resulting fit values for the lower energies are lower than those from the global fit, namely differing by $\Delta T_{\mathrm{low}} = -70$ K and $\Delta D_{\mathrm{low}} = -0.2$ eV. The fit values from the higher energies, on the other hand, stay within the uncertainties of the global fit ($\Delta T_{\mathrm{high}} < 20$ K and $\Delta D_{\mathrm{high}} < 0.1$ eV). The small deviations indicate a very robust fitting procedure.

While the low- and high-energy fits are performed using half of the available data, respectively, curves for both of these fits are drawn for all photon energies in Fig. 4 for easier comparison. For these additional curves, the k-distributions are calculated by using the fit results for temperature T and dissociation energy D of the high-energy and low-energy fit, respectively, while only the amplitudes are fitted to the data.

As an additional parameter for goodness-of-fit evaluation, the χ_r^2 values are compared. The global fit produces a reduced-chi-squared value of $\chi_\mathrm{r}^2 = 2.2$. The high-energy fit is nearly identical with a small increase of $\Delta\chi_{\mathrm{r,high}}^2 < 0.01$, while the low-energy fit deviates slightly with an increase of $\Delta\chi_{\mathrm{r,low}}^2 = 0.4$. This is also visible in Fig. 4, where the curves from the low-energy fits deviate somewhat from those of the highest energies. Nevertheless, the fits are in good agreement, suggesting a reliable overall result.

The width of the k-distributions σ_k decreases with increasing photon energy, as seen in Fig. 4. This suggests that for increasingly higher photon energies with respect to the dissociation energy, the fragment yields can eventually be approximated by a single exponential function, if the experimental observation window of the delay time allows it. Indeed, this was the case in the early days of the ClusterTrap measurements more than two decades ago.[3,40–42,51] In contrast, as demonstrated by Fig. 2, the present case is more complex and calls for a more detailed approach such as the one presented here.

Note that, in general, the experiment-specific observation-time window limits the photon energies that can be probed. For broad k-distributions this limit can be a severe problem, as data points from an extended delay-time range are needed to fully describe the time-dependent fragment yield. The obvious solution to this problem would be to adjust, specifically to lower, the initial temperature of the cluster ensemble. This is not possible at the present setup. However, it should also be noted that the dissociation energy can be determined without extended modeling as well, namely in cases where sequential decays can be characterized by a photon-energy dependent parameter. This can be, e.g., competing decay pathways,[52] but also delayed decays.[53] For the latter, the particular parameter characterizing the decay curve is not essential, as long as the determination is performed consistently. In the present case, the intensity of the excitation laser pulse was, however, not high enough to observe the sequential decay of Sn$_{22}^-$ via Sn$_{15}^-$ to smaller clusters, which prevented the application of this method.

Density-Functional-Theory (DFT) calculations by Wiesel et al.[22] found a dissociation energy for Sn$_{22}^-$ of $D_{\mathrm{DFT}} = 1.0$ eV, i.e. considerably lower than the present result. In the same work, collision-induced-dissociation measurements have shown several different decay channels with Sn$_{15}^-$ being the most prominent. In the present work, the comparatively low photon energies of the photodissociation yielded the observation of only Sn$_{15}^-$ fragments, which confirms it as the lowest-energy decay channel for this cluster size.

In other investigations, the electron affinity EA(n) of Sn$_7$ and Sn$_{15}$ have been measured by Negishi et al.[18] and Cui et al.[19] by photo-electron-spectroscopy. Both report considerably higher electron affinities for Sn$_{15}$ than Sn$_7$ at EA$_{\mathrm{Negishi}}$(7) $= 1.87(7)$ eV and EA$_{\mathrm{Negishi}}$(15) $= 2.66(4)$ eV, and EA$_{\mathrm{Cui}}$(7) $= 2.10(7)$ eV and EA$_{\mathrm{Cui}}$(15) $= 2.97(5)$ eV, respectively. This aligns with the finding in the present work, as the charged Sn$_7^-$ fragment is not observed, indicating a very strong statistical preference of the excess electron to stay attached to the Sn$_{15}^-$ fragment.

5 Summary and conclusion

The delayed decay of the tin cluster Sn$_{22}^-$ after photoexcitation has been measured. The abundance of the product fragment Sn$_{15}^-$ is monitored with respect to the delay time and photon energy. In contrast to previous experiments with the same apparatus, the data analysis requires that distributions of decay constants are considered. One reason for the importance of the spread in rate constants in the present work can be traced to the small dissociation energy, which increases the impact of

This journal is © the Owner Societies 2024

Phys. Chem. Chem. Phys., 2024, 26, 1105–1112 | 1109

the thermal energy contribution and its width compared to more stable species. A simultaneous fit of the delayed fragment yields for multiple photon energies has been applied. The resulting estimations for the internal energy of the cluster ensemble prior to the photoexcitation pulse is somewhat higher than room temperature, but still reasonably possible given that the charged clusters are exposed to buffer-gas collisions and radial excitation fields during their axialization in the Penning trap prior to the photoexcitation. The dissociation threshold resulting from the fits is the first report of this value for a small tin cluster derived from experimental data. The experimental value is a factor of two higher than the one from quantum chemical calculations.

Conflicts of interest

There are no conflicts to declare.

Appendix

The decay-constant distribution

Calculating the distributions of decay constants $\rho(k)\mathrm{d}k$ requires the underlying energy distribution of the cluster ensemble and an expression for the energy dependence of the cluster decay constant. In the present study the tin cluster Sn_{22}^- is described as a collection of f harmonic oscillators, where

$$f = 3n - 6 = 60, \tag{8}$$

is the number of vibrational degrees of freedom for the cluster size $n = 22$. The clusters are assumed to be a thermalized ensemble in the trap prior to the photoexcitation. In the high temperature limit of harmonic oscillators the initial energy distribution $\rho(E_{\mathrm{ini}})\mathrm{d}E_{\mathrm{ini}}$ is[54]

$$\rho(E_{\mathrm{ini}})\mathrm{d}E_{\mathrm{ini}} = \frac{(E_{\mathrm{ini}} + E_{0,\mathrm{p}})^{f-1}}{\Gamma(f)(k_{\mathrm{B}}T)^f} \, \mathrm{e}^{-\frac{E_{\mathrm{int}} + E_{0,\mathrm{p}}}{k_{\mathrm{B}}T}} \mathrm{d}E_{\mathrm{ini}}, \tag{9}$$

where $\Gamma(f)$ is the gamma function and k_{B} is the Boltzmann constant, and

$$E_{0,\mathrm{p}} = \frac{3}{8}f k_{\mathrm{B}} T_{\mathrm{D}} = 0.37 \text{ eV} \tag{10}$$

is the offset of the caloric curve in the Debye model. Here $T_{\mathrm{D}} = 200$ K is the Debye-temperature of bulk tin.[55] The distribution can be approximated by a Gaussian function

$$\rho(E_{\mathrm{ini}})\mathrm{d}E_{\mathrm{ini}} = \frac{1}{\sqrt{2\pi f(k_{\mathrm{B}}T)^2}}$$
$$\times \exp\left(-\frac{(E_{\mathrm{ini}} + E_{0,\mathrm{p}} - f k_{\mathrm{B}}T)^2}{2f(k_{\mathrm{B}}T)^2}\right)\mathrm{d}E_{\mathrm{ini}}. \tag{11}$$

We do not distinguish between a canonical ensemble ($f k_{\mathrm{B}}T$) and a micro-canonical ensemble (($f - 1)k_{\mathrm{B}}T$) in the two denominators. To convert the energy distribution to a decay constant distribution, an Arrhenius-like expression is applied.[56,57] The detailed balance expression involves the ratio

of the product and the precursor level densities. It can be approximated by an exponential. The value of the argument is calculated in detail in.[56] The leading order approximation, with the modifications required for the loss of a polyatomic fragment with its own vibrational degrees of freedom, is

$$k(E) = \omega \exp\left(-\frac{D + E_{0,\mathrm{p}} - E_{0,\mathrm{f}}}{E + E_{0,\mathrm{p}} - D/2}(f - 4)\right), \tag{12}$$

where D is the dissociation energy and $E_{0,\mathrm{f}}$ is the offset of the caloric curve for the fragment cluster and is defined analogous to $E_{0,\mathrm{p}}$. The difference $E_{0,\mathrm{p}} - E_{0,\mathrm{f}}$ amounts to the loss of vibrational zero point energy during the fragmentation and is equal to $6 \times 3/8 \times k_{\mathrm{B}}T_{\mathrm{D}}$. The term $D/2$ in (12) is the leading order finite-heat-bath correction.[57] The frequency factor ω can be expressed as

$$\omega = \omega_{\mathrm{D}} \times 100 \times n^{2/3}, \tag{13}$$

where

$$\omega_{\mathrm{D}} = \frac{k_{\mathrm{B}}T_{\mathrm{D}}}{\hbar} = 26 \times 10^{12}\,\mathrm{s}^{-1} \tag{14}$$

is the Debye frequency of tin. The factor of 100 is derived from fits of bulk vapor pressures for 13 of elements and does not specifically refer to tin or to the tin heptamer.[57] The frequency factor used here does not include the rotational degrees of freedom created in the fragmentation. A quantitative estimation for these could not be provided here. The $n^{2/3}$ represents the variation of the surface area with size. The form of the rate constant is justified by a rewrite of the detailed balance rate constant. The details require some space and can be found elsewhere.[56,57] The energy E in eqn (12) is substituted by a linear approximation of the Debye model for the caloric curve at high temperatures including the photon energy absorbed by the cluster during photoexcitation,[56]

$$E = E_{\mathrm{ph}} + f k_{\mathrm{B}}T - E_{0,\mathrm{p}}. \tag{15}$$

To convert the energy distribution into a k-distribution, the Gaussian approximation for the initial thermal source distribution is used. With the previously given expressions and definitions of the constants and a saddle point expansion the decay-constant distribution becomes

$$\rho(k)\mathrm{d}k = \frac{1}{\sqrt{2\pi\sigma_{\mathrm{k}}^2 k^{-1}}} \exp\left(-\frac{1}{2\sigma_{\mathrm{k}}^2}\left(\ln\frac{k}{k_{\mathrm{m}}}\right)^2\right)\mathrm{d}k. \tag{16}$$

Here,

$$k_{\mathrm{m}} = \omega \exp\left(-\frac{(D + E_{0,\mathrm{p}} - E_{0,\mathrm{f}})(f - 4)}{E_{\mathrm{ph}} - D/2 + f k_{\mathrm{B}}T}\right). \tag{17}$$

is the median decay constant and

$$\sigma_{\mathrm{k}} = \frac{(D + E_{0,\mathrm{p}} - E_{0,\mathrm{f}})(f - 4)\sqrt{f}k_{\mathrm{B}}T}{(E_{\mathrm{ph}} - D/2 + f k_{\mathrm{B}}T)^2}, \tag{18}$$

is the width of the distribution.

1110 | *Phys. Chem. Chem. Phys.*, 2024, **26**, 1105–1112

This journal is © the Owner Societies 2024

References

1 C. Bréchignac, P. Cahuzac, F. Carlier, M. de Frutos and J. Leygnier, Alkali-metal clusters as prototypes of metal clusters, *J. Chem. Soc., Faraday Trans.*, 1990, **86**(13), 2525–2531.

2 S. Nonose, H. Tanaka, T. Mizuno, J. Hirokawa and T. Kondow, Role of electron pairing in collisional dissociation of Na_9^+ by a rare-gas atom, *J. Chem. Phys.*, 1996, **104**, 5869–5874.

3 M. Vogel, A. Herlert and L. Schweikhard, Photodissociation of Small Group-11 Metal Cluster Ions: Fragmentation Pathways and Photoabsorption Cross Sections, *J. Am. Soc. Mass Spectrom.*, 2003, **14**, 614–621.

4 A. A. Shvartsburg and M. F. Jarrold, Transition from covalent to metallic behavior in group-14 clusters, *Chem. Phys. Lett.*, 2000, **317**, 615–618.

5 M. E. Geusic, M. F. Jarrold, T. J. McIlrath, R. R. Freeman and W. L. Brown, Photodissociation of carbon cluster cations, *J. Chem. Phys.*, 1987, **86**, 3862–3869.

6 M. J. Deluca and M. A. Johnson, Photofragmentation of C_n^-, $4 \leq n \leq 20$: Loss of neutral C_3, *Chem. Phys. Lett.*, 1988, **152**, 67–70.

7 B. Pozniak and R. C. Dunbar, Photodissociation and photodetachment of small carbon cluster anions, *Int. J. Mass Spectrom. Ion Processes*, 1994, **133**, 97–110.

8 B. P. Pozniak and R. C. Dunbar, Photodissociation studies of C_n^+ at 193 nm (n = 5–19), *Int. J. Mass Spectrom. Ion Processes*, 1997, **165–166**, 299–313.

9 L. A. Bloomfield, R. R. Freeman and W. L. Brown, Photofragmentation of Mass-Resolved Si_2-12^+ Clusters, *Phys. Rev. Lett.*, 1985, **54**, 2246–2249.

10 M. F. Jarrold and J. E. Bower, Collision-induced dissociation of silicon cluster ions, *J. Phys. Chem.*, 1988, **92**, 5702–5705.

11 Y. Liu, Q.-L. Zhang, F. K. Tittel, R. F. Curl and R. E. Smalley, Photodetachment and photofragmentation studies of semiconductor cluster anions, *J. Chem. Phys.*, 1986, **85**, 7434–7441.

12 Q.-L. Zhang, Y. Liu, R. F. Curl, F. K. Tittel and R. E. Smalley, Photodissociation of semiconductor positive cluster ions, *J. Chem. Phys.*, 1988, **88**, 1670–1677.

13 P. Ferrari, E. Janssens, P. Lievens and K. Hansen, Thermal radiation and fragmentation pathways of photo-excited silicon clusters, *J. Chem. Phys.*, 2015, **143**, 224313.

14 A. Lehr, F. Rivic, M. Jäger, M. Gleditzsch and R. Schäfer, Optical absorption and shape transition in neutral Sn_N clusters with $N \leq 40$: a photodissociation spectroscopy and electric beam deflection study, *Phys. Chem. Chem. Phys.*, 2022, **24**(19), 11616–11635.

15 S. Yoshida and K. Fuke, Photoionization studies of germanium and tin clusters in the energy region of 5.0–8.8 eV: Ionization potentials for Ge_n (n = 2–57) and Sn_n (n = 2–41), *J. Chem. Phys.*, 1999, **111**, 3880–3890.

16 G. Ganteför, M. Gausa, K. H. Meiwes-Broer and H. O. Lutz, Photoemission from tin and lead cluster anions, *Z. Phys. D: At., Mol. Clusters*, 1989, **12**, 405–409.

17 V. D. Moravec, S. A. Klopcic and C. C. Jarrold, Anion photoelectron spectroscopy of small tin clusters, *J. Chem. Phys.*, 1999, **110**, 5079–5088.

18 Y. Negishi, H. Kawamata, A. Nakajima and K. Kaya, Photoelectron spectroscopy of tin and lead cluster anions: application of halogen-doping method, *J. Electron Spectrosc. Relat. Phenom.*, 2000, **106**, 117–125.

19 L.-F. Cui, L.-M. Wang and L.-S. Wang, Evolution of the electronic properties of Sn_n^- clusters (n = 4–45) and the semiconductor-to-metal transition, *J. Chem. Phys.*, 2007, **126**, 064505.

20 E. Oger, R. Kelting, P. Weis, A. Lechtken, D. Schooss, N. R. M. Crawford, R. Ahlrichs and M. M. Kappes, Small tin cluster anions: Transition from quasispherical to prolate structures, *J. Chem. Phys.*, 2009, **130**, 124305.

21 N. Drebov, E. Oger, T. Rapps, R. Kelting, D. Schooss, P. Weis, M. M. Kappes and R. Ahlrichs, Structures of tin cluster cations Sn_3^+ to Sn_{15}^+, *J. Chem. Phys.*, 2010, **133**, 224302.

22 A. Wiesel, N. Drebov, T. Rapps, R. Ahlrichs, U. Schwarz, R. Kelting, P. Weis, M. M. Kappes and D. Schooss, Structures of medium sized tin cluster anions, *Phys. Chem. Chem. Phys.*, 2012, **14**(1), 234–245.

23 A. A. Shvartsburg and M. F. Jarrold, Tin clusters adopt prolate geometries, *Phys. Rev. A: At., Mol., Opt. Phys.*, 1999, **60**, 1235–1239.

24 A. A. Shvartsburg and M. F. Jarrold, Solid Clusters above the Bulk Melting Point, *Phys. Rev. Lett.*, 2000, **85**, 2530–2532.

25 Y. Tai, J. Murakami, C. Majumder, V. Kumar, H. Mizuseki and Y. Kawazoe, Fragmentation of small tin cluster ions (Sn_x^+: x = 4–20) in the low-energy collisions with a highly oriented pyrolytic graphite surface, *J. Chem. Phys.*, 2002, **117**, 4317–4322.

26 H. Li, H. Du, W. Chen, Q. Q. Shan, Q. Sun, Z. X. Guo and Y. Jia, Threadlike Tin Clusters with High Thermal Stability Based on Fundamental Units, *J. Phys. Chem. C*, 2011, **116**, 231–236.

27 H. Li, W. Chen, F. Wang, Q. Sun, Z. X. Guo and Y. Jia, Tin clusters formed by fundamental units: a potential way to assemble tin nanowires, *Phys. Chem. Chem. Phys.*, 2013, **15**(6), 1831–1836.

28 D. Wu, Q. Du, X. Wu, R. Shi, L. Sai, X. Liang, X. Huang and J. Zhao, Evolution of atomic structures of Sn_N, Sn_N^-, and SnNCl− clusters (N = 4–20): Insight from *ab initio* calculations, *J. Chem. Phys.*, 2019, **150**, 174304.

29 C. Majumder, V. Kumar, H. Mizuseki and Y. Kawazoe, Small clusters of tin: Atomic structures, energetics, and fragmentation behavior, *Phys. Rev. B: Condens. Matter Mater. Phys.*, 2001, **64**, 233405.

30 P. Jackson, I. G. Dance, K. J. Fisher, G. D. Willett and G. E. Gadd, Mass spectrometry and density functional studies of neutral and anionic tin clusters, *Int. J. Mass Spectrom. Ion Processes*, 1996, **157–158**, 329–343.

31 K. Joshi, D. G. Kanhere and S. A. Blundell, Thermodynamics of tin clusters, *Phys. Rev. B: Condens. Matter Mater. Phys.*, 2003, **67**, 235413.

This journal is © the Owner Societies 2024

Phys. Chem. Chem. Phys., 2024, **26**, 1105–1112 | **1111**

32 S. König, A. Jankowski, G. Marx, L. Schweikhard and M. Wolfram, Fission of Polyanionic Metal Clusters, *Phys. Rev. Lett.*, 2018, **120**, 163001.

33 M. Wolfram, S. Bandelow, A. Jankowski, S. König, G. Marx and L. Schweikhard, Photodissociation of mono- and di-anionic tin clusters, *Eur. Phys. J. D*, 2020, **74**, 135.

34 Y. Tao, H. Nishimura, T. Okuno, S. Fujioka, N. Ueda, M. Nakai, K. Nagai, T. Norimatsu, N. Miyanaga, K. Nishihara and Y. Izawa, Dynamic imaging of 13.5 nm extreme ultraviolet emission from laser-produced Sn plasmas, *Appl. Phys. Lett.*, 2005, **87**, 241502.

35 A. Herlert and L. Schweikhard, Delayed neutral-atom evaporation of photoexcited anionic gold clusters, *Int. J. Mass Spectrom.*, 2006, **249–250**, 215–221.

36 M. Wolfram, S. König, S. Bandelow, P. Fischer, A. Jankowski, G. Marx and L. Schweikhard, Disentangling the photodissociation pathways of small lead clusters by time-resolved monitoring of their delayed decays: the case of Pb_{31}^{+}, *J. Phys. B*, 2018, **51**, 044005.

37 L. Schweikhard, S. Krückeberg, K. Lützenkirchen and C. Walther, The Mainz cluster trap, *Eur. Phys. J. D*, 1999, **9**, 15–20.

38 F. Martinez, S. Bandelow, C. Breitenfeldt, G. Marx, L. Schweikhard, A. Vass and F. Wienholtz, Upgrades at ClusterTrap and Latest Results, *Int. J. Mass Spectrom.*, 2014, **365–366**, 266–274.

39 M. Vogel, K. Hansen, A. Herlert and L. Schweikhard, Decay pathways of small gold clusters, *Eur. Phys. J. D*, 2001, **16**, 73–76.

40 U. Hild, G. Dietrich, S. Krückeberg, M. Lindinger, K. Lützenkirchen, L. Schweikhard, C. Walther and J. Ziegler, Time-resolved photofragmentation of stored silver clusters Ag_n^{+} ($n = 8$–21), *Phys. Rev. A: At., Mol., Opt. Phys.*, 1998, **57**, 2786–2793.

41 C. Walther, G. Dietrich, W. Dostal, K. Hansen, S. Krückeberg, K. Lützenkirchen and L. Schweikhard, Radiative Cooling of a Small Metal Cluster: The Case of V_{13}^{+}, *Phys. Rev. Lett.*, 1999, **83**, 3816–3819.

42 K. Hansen, A. Herlert, L. Schweikhard, M. Vogel and C. Walther, The dissociation energy of V_{13}^{+} and the consequences for radiative cooling, *Eur. Phys. J. D*, 2005, **34**, 67–71.

43 H. Weidele, U. Frenzel, T. Leisner and D. Kreisle, Production of Cold/Hot Metal Cluster Ions: a Modified Laser Vaporization Source, *Z. Phys. D: At. Mol. Clusters*, 1991, **20**, 411–412.

44 L. Schweikhard and A. G. Marshall, Excitation modes for Fourier transform-ion cyclotron resonance mass spectrometry, *J. Am. Soc. Mass Spectrom.*, 1993, **4**, 433–452.

45 G. Bollen, R. B. Moore, G. Savard and H. Stolzenberg, The accuracy of heavy-ion mass measurements using time of flight-ion cyclotron resonance in a Penning trap, *J. Appl. Phys.*, 1990, **68**, 4355–4374.

46 G. Savard, S. Becker, G. Bollen, H.-J. Kluge, R. B. Moore, T. Otto, L. Schweikhard, H. Stolzenberg and U. Wiess, A new cooling technique for heavy ions in a Penning trap, *Phys. Lett. A*, 1991, **158**, 247–252.

47 L. Schweikhard, S. Guan and A. G. Marshall, Quadrupolar excitation and collisional cooling for axialization and high pressure trapping of ions in Fourier transform ion cyclotron resonance mass spectrometry, *Int. J. Mass Spectrom. Ion Processes*, 1992, **120**, 71–83.

48 V. V. Kresin, Collective resonances and response properties of electrons in metal clusters, *Phys. Rep.*, 1992, **220**, 1–52.

49 C. Brechignac and J. P. Connerade, Giant resonances in free atoms and in clusters, *J. Phys. B: At., Mol. Opt. Phys.*, 1994, **27**, 3795–3828.

50 I. Vasiliev, S. Öğüt and J. R. Chelikowsky, *Ab Initio* Excitation Spectra and Collective Electronic Response in Atoms and Clusters, *Phys. Rev. Lett.*, 1999, **82**, 1919–1922.

51 (*a*) C. Walther, G. Dietrich, M. Lindinger, K. Lützenkirchen, L. Schweikhard and J. Ziegler, Time resolved photofragmentation of Au_{15}^{+} clusters, *Chem. Phys. Lett.*, 1996, **256**(1–2), 77–82; (*b*) C. Walther, G. Dietrich, M. Lindinger, K. Lützenkirchen, L. Schweikhard and J. Zieglers, Erratum: Time resolved photofragmentation of Au_{15}^{+} clusters, *Chem. Phys. Lett.*, 1996, **262**(5), 668.

52 M. Vogel, K. Hansen, A. Herlert and L. Schweikhard, Model-independent determination of dissociation energies: method and applications, *J. Phys. B: At., Mol. Opt. Phys.*, 2003, **36**, 1073–1083.

53 M. Vogel, K. Hansen, A. Herlert and L. Schweikhard, Model-Free Determination of Dissociation Energies of Polyatomic Systems, *Phys. Rev. Lett.*, 2001, **87**, 013401.

54 P. Fischer and L. Schweikhard, Decay-rate power-law exponent as a link between dissociation energy and temperature, *Phys. Rev. Res.*, 2020, **2**, 043177.

55 C. Kittel, *Introduction to solid state physics*. John Wiley and Sons, 2018.

56 K. Hansen, Decay dynamics in molecular beams, *Mass Spectrom. Rev.*, 2020, **40**, 725–740.

57 K. Hansen, *Statistical Physics of Nanoparticles in the Gas Phase*, Springer International Publishing, 2018.

1112 | *Phys. Chem. Chem. Phys.*, 2024, **26**, 1105–1112

This journal is © the Owner Societies 2024